

Electronic structure of $Y_{1-x}Ca_xVO_3$ studied by high-energy spectroscopies

H. F. Pen, M. Abbate,* A. Fujimori,[†] Y. Tokura,[‡] H. Eisaki,[§] S. Uchida,[§] and G. A. Sawatzky
*Laboratory of Applied and Solid State Physics, Materials Science Centre, University of Groningen,
 Nijenborgh 4, 9747 AG Groningen, the Netherlands*

(Received 29 May 1998)

We have studied the electronic structure of $Y_{1-x}Ca_xVO_3$ by x-ray-absorption and resonant photoemission spectroscopy. Upon hole doping the parent Mott-Hubbard insulator YVO_3 , an insulator-metal transition occurs at around $x \approx 0.5$. Resonant V $3p$ photoemission spectroscopy shows that the states near the Fermi level are of predominantly V $3d$ character; in $CaVO_3$, a Fermi edge is present. In the oxygen $1s$ x-ray-absorption spectra, the hole doping is reflected in a large increase of the spectral weight near threshold. Because large changes also appear in the vanadium $2p$ absorption edge, we conclude that the doped holes are of mixed O and V character. The results also indicate that the amount of O character increases with doping. The development of the photoemission and x-ray-absorption spectral weight differs from the rigid-band-like behavior predicted by one-electron band theory or Hubbard-model calculations. Our O $1s$ x-ray-absorption spectra show good correspondence with the optical spectra, indicating that interband features in the optical spectra are attributed to O $2p$ to V $3d$ charge-transfer excitations. [S0163-1829(98)03347-5]

I. INTRODUCTION

An important aspect of the electronic structure of transition metal oxides is the effect of doping. The high- T_c superconductivity in layered cuprates,¹ the colossal magnetoresistance in manganese oxides,^{2,3} and the peculiar phase transition in $(V_{1-x}Cr_x)_2O_3$ (Ref. 4) show that doping of the parent Mott-Hubbard or charge transfer compounds can lead to unexpected and interesting physical properties.

In this paper we study the electronic structure of the $Y_{1-x}Ca_xVO_3$ series using valence-band photoemission (PES) and x-ray-absorption spectroscopy (XAS). Compounds with the perovskite structure (AMO_3) are important model systems for studying the problem of doping in a systematic way. They contain MO_3 arrays that form corner-shared MO_6 octahedra. The oxidation state of the MO_3 arrays can be varied by taking A cations (usually rare-earth or alkali metal ions) with different valences, while the O coordination of the transition-metal ion M remains unchanged. The amount of doping can be changed in a continuous way, because many perovskites form solid solutions in a wide range of concentrations. The doping dependence of $Y_{1-x}Ca_xVO_3$ is particularly interesting because of the change from a Mott-Hubbard insulator, YVO_3 , to a “correlated” metal, $CaVO_3$. PES and XAS have proven to be useful tools for studying the electronic structure, in particular the doping dependence, of transition-metal oxides.⁵⁻⁹ The experimental spectra will be compared to the results of cluster and band-structure calculations.

There can be several “side effects” of the change in composition, for example a change in the V $3d$ -band-width. The radius of the A ion is sometimes too large or too small to fit well at the A site, which leads to a distortion from the ideal cubic to the orthorhombic $GdFeO_3$ structure. The M -O- M bond angle θ becomes smaller than 180° , and the V $3d$ -band-width $W \propto |\cos \theta|$ is reduced.⁵ (Tight-binding calculations involving O $2p$ and TM $3d$ bands in the distorted

perovskite structure¹⁰ show indeed a $W \propto |\cos \theta|$ behavior, and not $W \propto \cos^2 \theta$ as suggested in Ref. 11.) Another effect is the decrease of the charge-transfer energy with increasing M -ion valence, due to changes in ionization and Madelung potentials.¹²

In $Y_{1-x}Ca_xVO_3$, the nominal V valence is changed from 3^+ ($x=0$, d^2) to 4^+ ($x=1$, d^1). An insulator-metal transition occurs at around $x \approx 0.5$. YVO_3 is an antiferromagnetic (AFM) insulator with an optical band gap of ~ 1.2 eV.¹³ The magnetic behavior is complicated: the spin structure is G -type AFM below 77 K, C -type AFM between 77 and 118 K, and paramagnetic above 118 K.^{14,15} The properties of $CaVO_3$ are less clear. It has been reported metallic¹⁶⁻¹⁹ and insulating,^{13,20} Pauli paramagnetic,¹⁶ and Curie-Weiss paramagnetic.^{17,18} This large variation in properties reflects problems with oxygen stoichiometry. For example, the Curie-Weiss paramagnetic sample¹⁷ was an oxygen-deficient single crystal. After annealing in air at 450 K the sample became oxygen stoichiometric, according to thermogravimetric analysis, and it showed a Pauli paramagnetic behavior. On annealing in air above 900 K a phase transition to insulating CaV_2O_7 occurs. Nguyen and Goodenough also reported Pauli paramagnetism below 390 K.¹⁸ At 390 K, a first-order phase transition occurs and the high-temperature susceptibility obeys the Curie-Weiss law. This behavior is just opposite to that of Ref. 17; however, the measurements of Ref. 18 were carried out in vacuum, so the oxygen content of the samples is probably different in the two experiments. On the whole, we are convinced that (nearly) stoichiometric $CaVO_3$ is metallic, and that the magnetic susceptibility is almost temperature-independent between 100 and 400 K.

$CaVO_3$ has recently gained a lot of interest.^{5,21-23} Most studies were performed in the context of the properties of d^1 systems, in particular their dependence on the ratio of the on-site Coulomb repulsion U and the $3d$ -band-width W .^{6,24} The photoemission and optical conductivity spectra of these compounds have been described by the paramagnetic

solution of the $d=\infty$ Hubbard model;^{25–27} this will be discussed in some more detail in Sec. IV A. Heat-capacity measurements^{28,29} indicate an enhancement of the effective carrier mass m^* near the insulator-metal transition, suggesting the importance of on-site electron correlations for the transition.³⁰ The enhancement factor $m^*/m_b \approx 4$, where m_b is the local-density-approximation (LDA) band mass, is in reasonable agreement with photoemission. Using a phenomenological description of the photoemission spectrum, including the k and ω dependences of the self-energy, Inoue *et al.* found a similar mass enhancement ($m^*/m_b \approx 3$) in $Ca_{1-x}Sr_xVO_3$.⁵

Kasuya *et al.* measured the optical conductivity of the $Y_{1-x}Ca_xVO_3$ series and found for YVO_3 , a thresholdlike intensity increase around $\omega = 1.5$ eV, which was attributed to the Mott-Hubbard gap.¹⁹ On doping, spectral weight appears below 1.5 eV, gradually replacing the upper Hubbard band and showing Drude-like behavior in the metallic regime.

II. EXPERIMENTAL DETAILS

Polycrystalline samples of $Y_{1-x}Ca_xVO_3$, with compositions between $x=0.0$ and 1.0 , were melt grown using a floating-zone furnace. This method yields the high-density samples that are needed for surface sensitive techniques like PES and XAS. Details of the sample preparation are described elsewhere.¹⁹

The x-ray-absorption experiments were carried out at the Berlin synchrotron radiation source (BESSY), using the SX700-II monochromator.³¹ The resolution was about 0.3 eV. The spectra were recorded in total electron yield mode. They were normalized to the spectrum of clean Pt, to correct for the monochromator throughput (platinum does not have any absorption edge in the energy region considered here). Due to the indirect detection method, an absolute normalization of spectra from different samples is not possible. To compare the spectra for the different compositions, they were normalized to the intensities at 510 and 555 eV, where effects of doping are expected to be small: the first energy is below the V edge, the second is 25 eV above the O edge.

The photoemission measurements of the $x=0.0$ and 1.0 samples were performed at beam line 6.2 of SRS (Synchrotron Radiation Source, Daresbury), using a toroidal-grating monochromator.³² The photoelectrons were detected in a hemispherical analyzer, using the constant pass energy mode. The combined resolution of the monochromator and analyzer was approximately 0.5 eV. The photoemission measurements of samples with other compositions between $x=0.0$ and 1.0 were made using a He discharge lamp and a double-pass cylindrical mirror analyzer. All measurements were carried out in ultrahigh-vacuum chambers, with a pressure in the 10^{-8} Pa range. To remove surface contamination, the samples were scraped *in situ* with a diamond file. Several scans of different parts of the samples were taken to ensure reproducibility.

III. BAND-STRUCTURE CALCULATIONS

Local (spin) density [L(S)DA] calculations of $CaVO_3$ and YVO_3 were performed in the linearized muffin-tin orbitals (LMTO) approach.^{33,34} The atomic positions used in the cal-

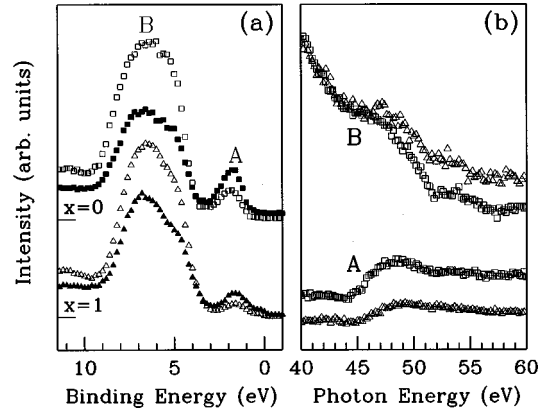


FIG. 1. (a) Vanadium 3*p* resonant photoemission of YVO_3 (squares) and $CaVO_3$ (triangles) at resonance ($\hbar\omega = 50$ eV, solid symbols) and off resonance ($\hbar\omega = 40$ eV, open symbols). (b) Constant initial state spectra of YVO_3 (squares) and $CaVO_3$ (triangles). The spectra are normalized to the off-resonance intensity (40–45 eV) of peak A.

culations correspond to those in the true orthorhombically distorted crystal structures.^{15,35} The basis set for the valence electrons consisted of 3*d*-, 4*s*-, and 4*p*-like basis functions for V; 3*s*-, 2*p*-, 3*d*-like for O; 5*s*-, 5*p*-, 4*d*-, and 4*f*-like for Y; and 4*s*-, 4*p*-, and 3*d*-like for Ca.

The densities of states were calculated with a Brillouin-zone integration over 125 irreducible \mathbf{k} points. In the LSDA calculation of YVO_3 , the symmetry of the unit cell was lowered, to allow for C-type AFM ordering. The calculated magnetic moment was $1.5\mu_B$, equal to that obtained from a Hartree-Fock band-structure calculation on C-type YVO_3 ,³⁶ but larger than the experimental value of $1.0\mu_B$.¹⁵ For $CaVO_3$, LSDA calculations for different magnetic orderings were tried, but in each case the local magnetic moment converged to zero during the calculation of the self-consistent potential.

In all calculations, either within the LDA or the LSDA approximation, the density of states at the Fermi energy remains finite. So the LMTO calculations predict both $CaVO_3$ and YVO_3 to be metallic. However, as stated above, YVO_3 is an insulator with a band gap of 1.2 eV,¹³ which indicates the importance of electron correlation effects in this material.

IV. RESULTS AND DISCUSSION

A. V 3*p* resonant photoemission

Figure 1 shows the valence-band resonant photoemission (RPES) spectra of $CaVO_3$ and YVO_3 at photon energies between 35 and 60 eV. Both the $CaVO_3$ and YVO_3 spectra show a relatively weak and narrow feature (A) between 0- and 3-eV binding energy, which is attributed to states of V 3*d* character. This assignment is supported by the increased intensity of peak A above 45-eV photon energy, which corresponds roughly to the onset of the V 3*p* x-ray-absorption edge. The V 3*d* electron emission is enhanced due to quantum interference between the direct photoemission process ($3p^6 3d^n + \hbar\omega \rightarrow 3p^6 3d^{n-1} + e$) and the virtual V $3p \rightarrow 3d$ excitation process, followed by a super Coster-Kronig decay ($3p^6 3d^n + \hbar\omega \rightarrow 3p^5 3d^{n+1} \rightarrow 3p^6 3d^{n-1} + e$). The more in-

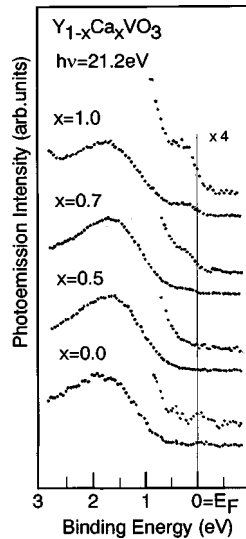


FIG. 2. Valence-band photoemission spectra of $Y_{1-x}Ca_xVO_3$ taken using the He I resonance line ($\hbar\omega = 21.2$ eV).

tense, broad band between 3- and 9-eV binding energy (B and C) is attributed to O $2p$ states.

The photon energy dependence of the spectral intensity is revealed more clearly in the constant initial state (CIS) spectra [Fig. 1(b)]. In this experiment, the difference between photon energy and electron kinetic energy was kept constant, to examine the resonance behavior of peaks labeled A and B in Fig. 1(a). The intensity of the V $3d$ band is enhanced by about a factor of 2 near the V $3p$ absorption threshold. The $3p$ resonance is quite weak and extends over a large energy range. This behavior seems to be typical for early transition-metal oxides, and is quite different from that in late transition-metal oxides, which show much narrower, Fano-like resonance profiles.^{37,38} The weight of the O $2p$ band decreases gradually with photon energy, in agreement with the change in the calculated atomic O $2p$ cross section.³⁹ A relatively small resonance is also seen for this band, due to the O $2p$ -V $3d$ hybridization. The RPES and CIS spectra of $CaVO_3$ and YVO_3 were normalized to the off-resonance intensity of the O $2p$ band. This yields a V $3d$ intensity that is twice as large for YVO_3 than for $CaVO_3$, as expected from the change in nominal valence. A remarkable difference between YVO_3 and $CaVO_3$ is the Fermi cutoff in the $CaVO_3$ spectra; it appears more pronounced in high-resolution measurements.¹¹ The evolution of the Fermi cutoff with Ca doping in $Y_{1-x}Ca_xVO_3$ is demonstrated in Fig. 2. It turns out to be present only in the metallic ($x > 0.5$) samples. We will discuss this in more detail later on.

In a one-electron band-structure picture, the photoemission spectrum corresponds to the density of states (DOS), weighted with the corresponding transition matrix elements, at least, if interference effects can be neglected. Furthermore, one has to take into account the experimental resolution and extrinsic electron-energy-loss processes. The band-structure calculation discussed in Sec. III treats electron correlation only approximately, and for correlated electron systems the calculated DOS has in principle no physical meaning. Nevertheless, it is tempting to make a comparison between band theory and PES of $CaVO_3$ and YVO_3 . It has been shown that the photoemission spectra of some late transition-metal

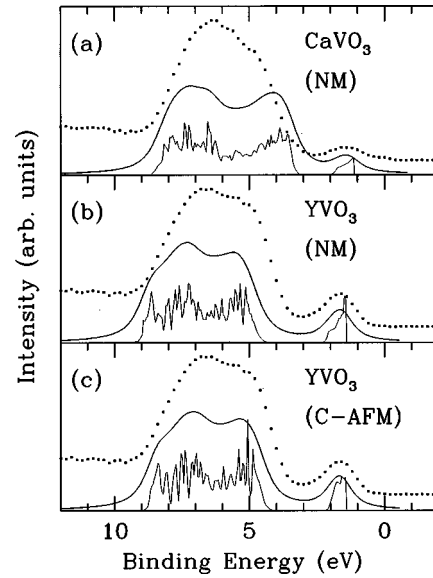


FIG. 3. Valence-band photoemission spectra of $CaVO_3$ (top panel) and YVO_3 (lower panels). The experimental spectra (dots) are compared to the DOS (solid lines) obtained from band-structure calculations. Also, the Gaussian-broadened DOS is shown for ease of comparison. (a) and (b) show nonmagnetic calculations, (c) shows a LSDA calculation for YVO_3 , with C-type AFM ordering.

(TM) oxides with the perovskite structure are in surprisingly good agreement with the densities of states, calculated in the LSDA approximation.⁴⁰ Furthermore, correlation effects in the vanadium oxides are expected to be weaker than for the late transition-metal oxides. First, the $3d$ electrons are less localized in early TM oxides, because the smaller nuclear charge yields a larger $3d$ orbital radius. An even more important aspect is the absence of multiplet effects in the final state for both $CaVO_3$ and YVO_3 .

Figure 3 compares the experimental valence band PE spectra, taken at $\hbar\omega = 50$ eV, to densities of states, obtained in the L(S)DA calculations. At this photon energy, the cross sections of O $2p$ and V $3d$ are comparable,³⁹ so we use the total occupied DOS for this comparison. To obtain the best match with the spectral features, the DOS were broadened by a Gaussian of 1.2-eV full width at half maximums (considerably larger than the experimental resolution of 0.5 eV). Furthermore, the calculated line shapes were—tentatively—shifted toward higher binding energy (1.1 eV for $CaVO_3$, 1.4 eV for YVO_3) to obtain a better match of the peak positions. The broad bands around 6 eV are of primarily O $2p$ character, and the narrow band around 1.5 eV is mainly V $3d$, in agreement with the RPES experiment. The calculated bandwidths and their *relative* positions also resemble the PE spectra quite well. The increasing spectral intensity at the high-binding-energy side is due to inelastically scattered photoelectrons. The DOS calculated for YVO_3 with C-AFM ordering [Fig. 3(c)] is slightly different from the nonmagnetic DOS [Fig. 3(b)]. This is revealed in the shape of the V $3d$ band and the relative positions of the O $2p$ and V $3d$ bands.

Very remarkable is the shift of spectral weight away from E_F , even for the metallic $CaVO_3$. The broadness of the V $3d$ band and the low spectral weight near E_F were already discussed by Egdell *et al.* for $LaVO_3$ in a study of the

$La_{1-x}Sr_xVO_3$ system.⁴¹ From the conductivity behavior of the insulating compounds, they were expected to exhibit Anderson localization;⁴² however, the localized states below the mobility edge were not observed in the insulating compounds. The absence of spectral weight at the Fermi level was attributed to a final-state effect. The presence of the photohole in the polarizable lattice would give rise to a lattice relaxation, shifting the V $3d$ feature to higher binding energy. The peak also becomes broadened due to lattice vibrations: this is the Franck-Condon effect. It was noted by Egdell *et al.* that the Franck-Condon broadening is expected to become less important on going toward metallic materials. Nevertheless, as in $Y_{1-x}Ca_xVO_3$, the width of the 1.5-eV peak does not change very much with doping. This was explained by the increasing intrinsic bandwidth, which would compensate for the decreasing Franck-Condon broadening. The study was only made for samples with $x < 0.3$, so it was not noticed that also in $SrVO_3$ most of the spectral weight appears around 1.5-eV binding energy.

It was pointed out that not only $SrVO_3$, but also several other metallic systems with a d^1 configuration show the typical double-peak structure.²⁴ The intensity of the near-edge ‘‘coherent’’ spectral weight, attributed to quasiparticle excitations or renormalized d -band states, would increase with decreasing U/W with respect to the ‘‘incoherent’’ higher energy feature. The latter is associated with the remnant of the lower Hubbard band. This behavior is quite different from what is obtained for a simple Hubbard model.^{43,44} In this Monte Carlo calculation for an 8×8 cluster with nearest-neighbor hopping, the upper and lower Hubbard bands shift quite rigidly toward E_F on decreasing U/W , and finally merge into a single band.

The transfer of spectral weight, suggested in Ref. 24, was recently studied in a more systematic way in $Ca_{1-x}Sr_xVO_3$.⁵ A photoemission study on this system, in which the U/W ratio is varied systematically due to the composition-dependent V-O-V bond angle, confirmed the presumptions of Ref. 24. The spectra show a transfer of spectral weight away from E_F on increasing U/W . This was explained with a model for the spectral function including a k - and ω -dependent self-energy $\Sigma(k, \omega)$. The variation in the $Ca_{1-x}Sr_xVO_3$ low-energy PES was compared to the ‘‘Pauli paramagnetic’’ solution (i.e., without magnetic order) of the $d = \infty$ -Hubbard model.^{45,46} (Note that the ‘‘bare’’ $d = \infty$ Hubbard model, like the $d = 2$ model, fails to describe spectral weight transfer on changing the number of d electrons.⁴⁷ Recently, the doping dependence of $SrTiO_{3-\delta}$ was discussed using a $d = \infty$ model including disorder;^{26,27} the impurity potential of 2.4 eV used in this model, is very large, though.) This solution is essentially different from that obtained from two-dimensional Monte Carlo calculations,^{43,44} because no antiferromagnetic correlations are present. It is obtained only if frustration is included, in the form of hopping to more distant neighbors. Ulmke *et al.* noted that without this frustration the results for $d = 2$ and $d = \infty$ are very similar.⁴⁸ In the $d = \infty$ Hubbard model, the assignment of the 1.5-eV photoemission peak is essentially different from that of Egdell *et al.*:⁴¹ it is attributed to the on-site Coulomb interaction rather than to polarization effects.

The electron removal spectra calculated for $d = \infty$ resemble the experimental results quite well, if they are suffi-

ciently broadened. However, there is a qualitative disagreement which became clear from a high-resolution (35 meV) PES experiment by Morikawa *et al.*¹¹ In the $d = \infty$ Hubbard model, the peak near E_F narrows with increasing U/W , but in the PES spectra the intensity decreases, while the line shape is very close to the calculated LDA DOS. This was attributed to the k dependence of the self-energy $\Sigma(k)$, due to the long-range Coulomb interaction, which is not captured by the $d = \infty$ Hubbard model. Morikawa *et al.* argued that this interaction is not completely screened, at least between nearest-neighbor V atoms, because the screening length can not be smaller than the average distance between the conduction electrons. Therefore, the width of the coherent band will remain finite as m_ω diverges. This bandwidth is of the order $\sim e^2/\epsilon d$, where ϵ is the optical dielectric constant and d is the average electron-electron distance. With $d \approx 4$ Å and $\epsilon \sim 3-5$, it is estimated at 0.5–1 eV, comparable to the observed width of the coherent part.

An interesting question is whether lattice polarization can still influence the photoemission spectrum in the metallic case. Photoemission spectra of semiconducting $Na_xV_2O_5$ (Ref. 49) and of the metallic $La_{0.1}Sr_{0.9}TiO_3$ (Ref. 6) also show V $3d$ -like peaks at more than 1-eV binding energy. Nevertheless, the number of d electrons is much smaller than in $CaVO_3$, and the long-range Coulomb interaction is expected to be less important for these materials. So in this case, the large binding energy is probably due to lattice relaxation. Because the photoemission process is fast, the lattice cannot relax to screen the photohole in the final state. In a ‘‘poor’’ metal (small carrier concentration n , large effective mass m^*) this effect may still be present: if the plasma frequency $\omega_p = \sqrt{4\pi n e^2/m}$ becomes smaller, the screening of the photohole by conduction electrons decreases.

It would be interesting to examine a mixed valence compound that changes from polaronic to metallic behavior on increasing the number of d electrons per TM ion from 0 to 1. (Unfortunately $La_xSr_{1-x}TiO_3$ is metallic up to x values as low as ~ 0.05 .) It seems unlikely that the peak at high energy will disappear immediately when such a system becomes just metallic, simply because the number of itinerant electrons is too small to screen the photohole completely. On the other hand, if the system becomes metallic and a Fermi surface is present, spectral weight at the Fermi level should also appear. To describe such a spectrum theoretically, one needs a model that captures, in a realistic way, Coulomb interactions, lattice polarization and hybridization at the same time; this is an extremely difficult, and until now, unsolvable problem. To conclude this discussion, it is interesting to note the suggestion of Nguyen, Zhou, and Goodenough,^{18,23} who proposed an electronic phase segregation in which regions with localized and itinerant electrons coexist. This would also give rise to a double-peak structure, because the electrons in ‘‘itinerant’’ regions are well screened and those in ‘‘localized’’ regions are less screened.

B. V $2p$ x-ray absorption

Figure 4 shows the V $2p$ absorption edges of the $Y_{1-x}Ca_xVO_3$ series. Upon doping with Ca, clear changes are observed in the shapes of the spectra, as well as in their energy positions. To show the latter effect more clearly, the

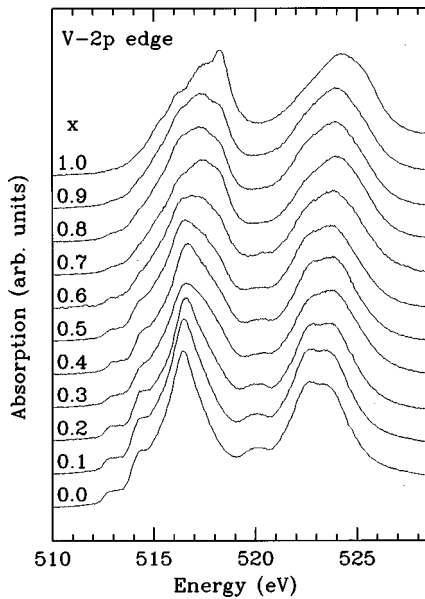


FIG. 4. Vanadium $2p$ absorption edges of $Y_{1-x}Ca_xVO_3$.

barycenters of the spectra [$E_b = \int EI(E)dE / \int I(E)dE$] are shown as a function of x in Fig. 5(a). On increasing x , the spectral weight gradually shifts toward higher energy. This “chemical shift” is attributed to a reduced final state screening, indicating an increasing average valence of the V ions. To examine the influence of the Ca doping in more detail, the experimental spectra were compared to calculations using the crystal-field multiplet model.⁵⁰ The V $2p$ line shape is very sensitive to the V ground state multiplet, and we can ask ourselves whether the change in d count, apparent from the energy shift, is reflected in the spectral shape. Therefore we performed several crystal-field multiplet calculations, varying the ground-state symmetry, the ionic crystal-field splitting $10Dq$, and the reduction of the Slater integrals.

In Figure 6(a) the V $2p$ spectrum of YVO_3 is compared to a multiplet calculation assuming a d^2 (3T_1) ground state, which turned out to give the best match. The Slater integrals were reduced to 70% of the Hartree-Fock values, and $10Dq$ was put at 1.5 eV. The sticks represent transitions to different final states. The solid line shows a simulated spectrum obtained by applying a convolution with a Lorentzian of 0.2 eV and a Gaussian of 0.3 eV, to account for lifetime and instrumental broadening. The agreement between experiment and calculation is very good. The main source of discrepancy is probably the nonuniformity of the lifetime broadening,

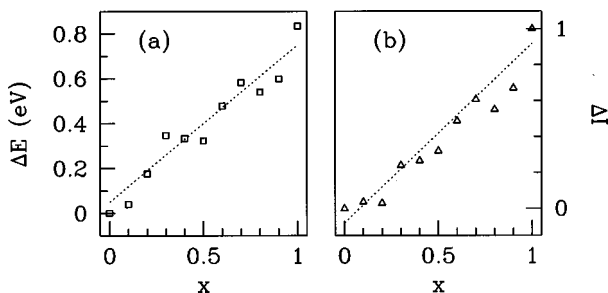


FIG. 5. Barycenter shift of the V $2p$ absorption edges (a), and growth of the 529-eV peak in the O $1s$ edges (b), both as a function of the hole doping x .

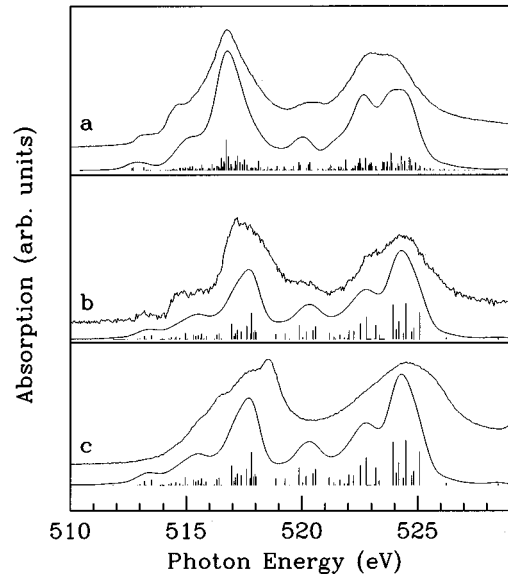


FIG. 6. Vanadium $2p$ spectra of $Y_{1-x}Ca_xVO_3$ compared to crystal-field multiplet calculations. (a) $x=0$ spectrum compared to a d^2 (3T_1) calculation. (b) “ d^1 ” part of the $x=0.1$ spectrum compared to a d^1 calculation. (c) $x=1.0$ spectrum compared to a d^1 calculation.

which could not be taken into account straightforwardly. The L_2 edge is relatively broad due to the additional Coster-Kronig decay channel, and also within the L_3 edge the higher-energy features appear broader. From the good agreement between the experiment and theoretical line shapes (and the large disagreement with line shapes calculated for other ground-state symmetries) we can conclude that the ground state of the V ion is indeed 3T_1 (d^2 , $S=1$). This is in accordance with magnetic-susceptibility measurements:⁵¹ in the paramagnetic phase a Curie-Weiss behavior is observed, with an effective magnetic moment $\mu_{\text{eff}}=3.11\mu_B$, close to the V^{3+} free-ion value of $2.8\mu_B$. Also, ${}^{51}\text{V}$ NMR experiments²⁸ support the presence of an $S=1$ moment at the V site.

Usually, YVO_3 is regarded as a typical Mott-Hubbard insulator. This implies that doped holes will reside on the TM ions: upon increasing x , the V^{3+} ions are gradually replaced by V^{4+} . To test this assumption, we subtracted appropriate fractions of the $x=0$ spectrum from the $x>0.0$ spectra, and compared the results to a V^{4+} (d^1) crystal-field multiplet calculation. The Slater integral reduction and $10Dq$ were taken as before. Figure 6(b) shows that the agreement is remarkably good for $x=0.1$: all major features are still reproduced. Therefore, we conclude that for small x values the V $2p$ XAS spectra can be described by a superposition of spectra corresponding to $3d^1$ and $3d^2$ ground states, as expected from the Mott-Hubbard picture. Note that the difference spectrum is shifted about 1 eV toward higher energy compared to the $x=0$ spectrum, consistent with the presence of V^{4+} ions. When comparing spectra of V_2O_3 and VO_2 , with nominal V valences of 3 and 4, respectively, a shift of the same magnitude is observed.⁵²

On increasing x , the agreement between the V $2p$ spectra and the multiplet calculations becomes increasingly poor. In Fig. 6(c), the $x=1$ spectrum is compared to the same d^1 calculation as shown in Fig. 6(b). The spectrum is very

broad, with only some shoulders in the L_3 edge. Compared to Fig. 6(b), it contains more weight at higher energy in both the L_2 and L_3 edges, which could be due to V ions with a $5+$ valence. This broadness, and the d^0 component, indicate a wider d band and larger valence fluctuations than in the $x=0$ case, suggesting itinerant electron behavior. Both effects weaken the validity of the crystal-field multiplet approximation. The first one causes the final state to be less localized, and the second invalidates the description of the ground state as a single atomic configuration. The first possibility is less likely: the Ti $2p$ edge of $SrTiO_3$, which is expected to have a $3d$ -band-width comparable to $CaVO_3$, is still described very well by the crystal-field multiplet theory.⁷ However, $SrTiO_3$ is an insulator with an optical band gap of as much as 3.2 eV,⁵³ and valence fluctuations are negligible. So the main cause of the discrepancy is probably the presence of itinerant electrons in $CaVO_3$. Most likely, a calculation with only one V ion is too small: one would have to consider larger clusters⁵⁴ to capture the qualitative physics of $CaVO_3$. It is also interesting to note the similarity of the $x=1$ spectrum to the L edge of metallic V, as measured by electron-energy-loss spectroscopy:⁵⁵ here the delocalization of the d electrons gives rise to a broad spectrum.⁵⁶ Finally, a hypothetical cause for the disagreement could be the orthorhombic distortion of the crystal structure, because in the calculation O_H symmetry is assumed. However, as the deviation from cubic symmetry decreases on going from $x=0$ to 1, this possibility can be ruled out.

In conclusion, the YVO_3 spectrum is well described by a d^2 multiplet calculation, and for small doping concentrations the spectra resemble a superposition of the theoretical d^2 and d^1 spectra. For larger doping, the agreement between experiment and calculations becomes less good. Together, the changes in the V $2p$ absorption edge indicate an increasing covalence upon hole doping.

C. O 1s x-ray absorption

Figure 7 shows the O 1s x-ray-absorption edges of the $Y_{1-x}Ca_xVO_3$ series. This edge probes the unoccupied states of O p character. Because in an ionic picture the O $2p$ shell would be completely filled, the absorption intensity is a direct measure of the degree of covalence. The near-edge intensity is in general attributed to states of mixed O $2p$ -V $3d$ character. The peaks at higher energy are assigned to Y $4d$ -Ca $3d$ (534–539 eV) and V $4s$ - $4p$ (534–550 eV). Probably, the contribution from Y $4d$ overlaps with that from V $3d$.

Upon doping, the spectra change drastically. The changes at higher energy can be attributed to band structure effects. The V $4s$ - $4p$ band shifts to higher energy, which can be related qualitatively to the decrease of the unit-cell volume, causing the unoccupied O $2p$ -V $4sp$ states to be more antibonding. Furthermore, we see a gradual decrease of the Y $4d$ structure and an increase of the Ca $3d$ structure. The most pronounced and also the most interesting changes, however, appear in the near-edge region. These changes are much too large to be explained by a rigid-band model: in this view, one would expect only a small increase in absorption, due to the increase of the number of holes in the V $3d$ band from 8

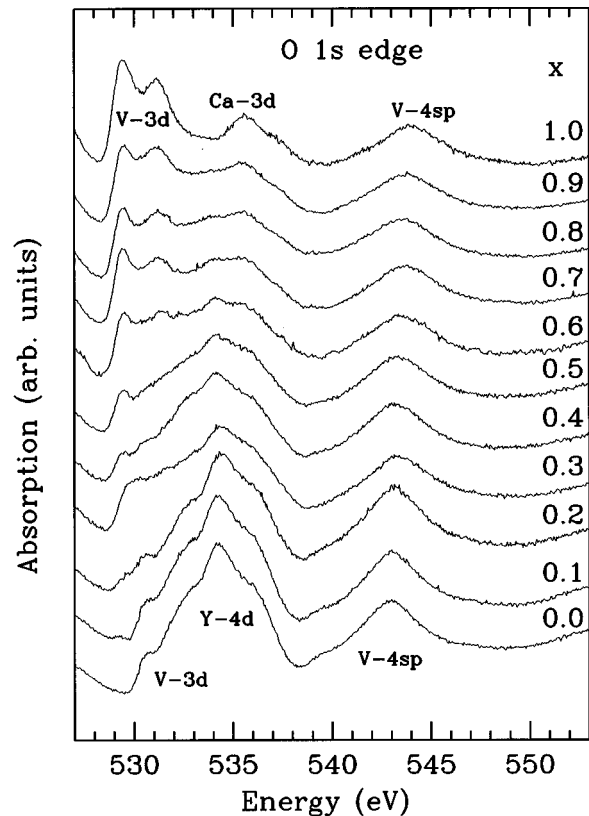


FIG. 7. Oxygen 1s absorption edges of $Y_{1-x}Ca_xVO_3$.

to 9. In contrast, the intensity around 534 eV decreases, and a pronounced double-peak structure starts to grow in the near-edge region.

Figure 5(b) shows the development of the 529-eV feature, i.e., the relative intensity $\Delta I(x) = [I(x) - I(x=0)] / [I(x=1) - I(x=0)]$ in a 1-eV window around the maximum of the 529-eV prepeak. The doping-induced changes in the O 1s spectra bear some similarities to those observed in the late transition metal oxides.^{9,57} The hole doping of YVO_3 results in an increasing intensity around 529 eV, which can be explained as the transfer of spectral weight to the lower Hubbard band. From the fact that these lower Hubbard band states are visible in O 1s XAS, combined with the observed changes in the V $2p$ XAS, we can conclude that they are of mixed V $3d$ -O $2p$ character. The increase of the peak intensity with x is approximately linear. This is different from the behavior in the late TM oxides, where a sublinear behavior is observed.⁵⁷ Also, in a “true” Mott-Hubbard insulator one would expect the transfer of spectral weight to the lower Hubbard band to be sublinear with the hole doping, due to hybridization.^{58,59} Probably the O $2p$ character of the holes—and thus the O 1s absorption intensity—increases on doping: the V $3d$ -O $2p$ covalence becomes larger, due to the increasing orbital overlap and the decreasing charge-transfer energy.

The O 1s absorption spectra of several TM oxides were described successfully by cluster model calculations.^{8,60,61} For YVO_3 , such a calculation was not possible due to the overlap between Y and V states, but for $CaVO_3$ we performed a cluster calculation for different values of the ionic crystal-field splitting ($10Dq$) and O $2p$ -V $3d$ hybridization. The observed double-peak structure could be simulated as-

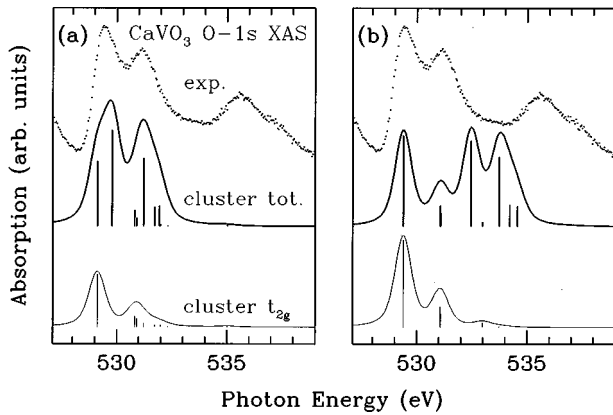


FIG. 8. O $1s$ absorption edge of CaVO_3 (dots), compared to cluster calculations with parameters $10Dq=0$, $(pd\sigma)=1.8$ eV in (a) and $10Dq=2.4$ eV, $(pd\sigma)=2.3$ eV in (b). The thick lines show the full cluster calculation, and the thin lines refer to states of t_{2g} symmetry.

suming $10Dq \approx 0$ and $(pd\sigma)=1.8$ eV [better agreement is found for smaller $(pd\sigma)$]. The resulting spectrum is shown in Fig. 8(a). The peak splitting would now be due to the ‘‘Hund’s rule’’ exchange splitting of about 1.6 eV between the lowest d^2 final-state multiplets. Although the spectrum calculated with these parameters is in good agreement with experiment, the values are much smaller than expected from band-structure calculations: from a tight-binding fit⁶² we obtain $(pd\sigma)=2.3$ eV and an ionic crystal-field splitting $10Dq=2.4$ eV. Figure 8(b) shows the calculation for these parameters. The agreement at higher energy is less good than in Fig. 8(a). However, the band-structure calculations show that the e_g band is very broad, which would ‘‘smear out’’ the final-state multiplets that involve e_g electrons. If this is the case, the sharp peaks in the spectrum would be due to final states involving t_{2g} electrons only. Like in Fig. 8(a), the peak splitting would now be due to the ‘‘Hund’s rule’’ exchange energy.

A different starting point for describing the O $1s$ XAS is the band-structure approach, comparing the spectra to the O p -projected unoccupied DOS.⁶³ In this picture, the observed splitting would be due to crystal-field effects: the octahedral surrounding of V by O splits the $3d$ band into bands of t_{2g} and e_g symmetry. Due to the large p - d hybridization, the e_g

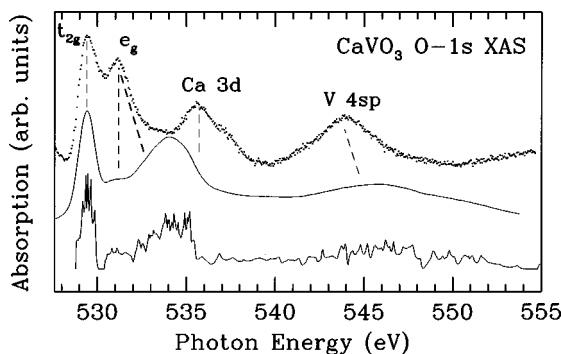


FIG. 9. O $1s$ absorption edges of CaVO_3 (dots), compared to the O p unoccupied DOS, as obtained by LDA band-structure calculations (solid lines). The dashed lines indicate the suggested connections between experimental and calculated features.

band is very wide, and does not induce a narrow feature in the unoccupied O p DOS, as is shown in Fig. 9. A similar disagreement in the comparison of SrTiO_3 O- $1s$ XAS to band-structure calculations was attributed to the core-hole effect.⁶ The presence of the O $1s$ core hole can redistribute spectral weight toward the lower band edges.^{63,64}

Figure 9 compares the experimental O $1s$ spectrum of CaVO_3 to the calculated O p -projected DOS. The DOS is shifted by 528.7 eV, so that the lowest-energy peaks of experiment and calculation coincide. To simulate the spectrum, the DOS is also broadened by Gaussian and Lorentzian line shapes. The differences can be largely explained by the neglect of the core-hole potential in the calculation. The core hole will pull spectral weight toward a narrow energy region near the lower edge of the t_{2g} and e_g bands. This will particularly affect the shape of the broad e_g band, because intensity is shifted from the region 532–535 eV toward the edge at 531 eV, as indicated by the thick dashed line in Fig. 9. The influence on the t_{2g} band will be much smaller because it is quite narrow (~ 1 eV from Fig. 9). The observed splitting is in good agreement with the distance of about 2.0 eV between the t_{2g} and e_g lower band edges. The description using the O p DOS, renormalized by the core hole, can also explain the difference between the O $1s$ XAS of CaVO_3 and SrVO_3 .²¹ In CaVO_3 , the second peak appears more pronounced. In the band structure of CaVO_3 , the e_g band is narrower, due to the orthorhombic distortion: this will enhance the effect of the core hole on the e_g DOS. An orbital projection of the DOS shows that the Ca $3d$ band is located between 4 and 8 eV above E_F , with a maximum DOS between 6 and 8 eV. This means that the calculation predicts the maximum of Ca $3d$ spectral weight between 535 and 537 eV, in good agreement with experiment. The V $4sp$ peak is less well described by the calculation; this is probably because the calculation becomes less accurate at energies high above E_F .

In conclusion, it is not clear whether the O $1s$ x-ray-absorption edge of CaVO_3 is best described in a band-structure or cluster approach. In the first case, we have to assume that the O $1s$ core hole has a considerable influence on the spectral shape. The splitting between the first two peaks would now be due to the crystal field. If the cluster approach is valid, the splitting would be due to the on-site exchange interaction. In this case, we must assume that any exchange splitting of final states involving e_g electrons is not visible in the spectrum, due to the broad e_g band. It is also possible that a combined approach is applicable here, with localized t_{2g} and delocalized e_g states.

Figure 10 compares the O $1s$ spectrum of YVO_3 to the O p projected DOS of LDA and LSDA calculations. As in Fig. 9, the DOS is shifted by 528.7 eV. As stated above, the doping dependence of O $1s$ XAS is not rigid-band-like. After concluding that the O $1s$ spectrum of CaVO_3 is described quite well by the O p DOS, it is therefore not surprising that in the case of YVO_3 the agreement is poor. Indeed, the DOS of the LDA calculation much resembles that of CaVO_3 , shown in Fig. 9, with a small shift due to the larger V $3d$ -band filling. The calculated near-edge intensity is much larger than observed. From the transfer of spectral weight upon doping it is clear that correlation effects are important

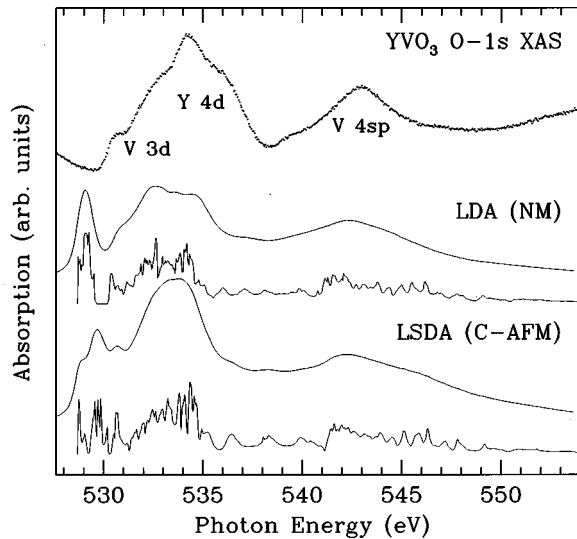


FIG. 10. O 1s absorption edges of YVO_3 (dots, top), compared to the O p unoccupied DOS, as obtained by LDA and LSDA band-structure calculations (solid lines).

for YVO_3 . The low near-edge spectral weight is better described by a calculation LSDA. This calculation assumes a two-sublattice structure, which allows for an AFM spin configuration. The essential improvement of the LSDA calculation is that it allows for the formation of local moments, which are present even in the paramagnetic phase of YVO_3 . With these local moments, the calculation can at least partially consider the on-site ‘‘Hund’s rule’’ exchange energy, which is important to give a correct description of the spectrum. The presence or absence of AFM is less important for the x-ray-absorption line shape, because the intersite exchange energy is much smaller than the on-site exchange energy. For these reasons, the LSDA calculation, with an AFM ground state, gives a better description of the XAS than the nonmagnetic LDA calculation, although the experimental spectrum was taken in the paramagnetic phase. It is not unlikely that the best agreement would—in principle—be obtained by a full multiplet calculation.

D. Optical conductivity and the $d=\infty$ Hubbard model

As we saw in the previous paragraphs, the photoemission spectrum of $CaVO_3$ is not well described in a delocalized (band structure) picture. Also, a localized description by a VO_6 cluster model does not give the correct result: the $d-d$ and $d-p$ interactions cannot give rise to a splitting of the lowest ($d^1 \rightarrow d^0$) electron removal state. $CaVO_3$ seems to represent a borderline case: the material is metallic, but correlation effects are still important. A theoretical approach to tackle this problem is the infinite-dimensional Hubbard model.²⁵ Recently, it was used to describe the photoemission spectra of $Ca_{1-x}Sr_xVO_3$.⁴⁵ In this series of compounds, the V-O-V bond angle is changing from 180° in $SrVO_3$ to 160° in $CaVO_3$. This leads to a systematic variation of the $3d$ -band-width W and the Coulomb energy U throughout the series. As discussed already in Sec. IV A, the low-energy parts of the photoemission spectra show a transfer of spectral weight toward the Fermi level on decreasing U/W . Similar changes are observed in the calculated electron removal

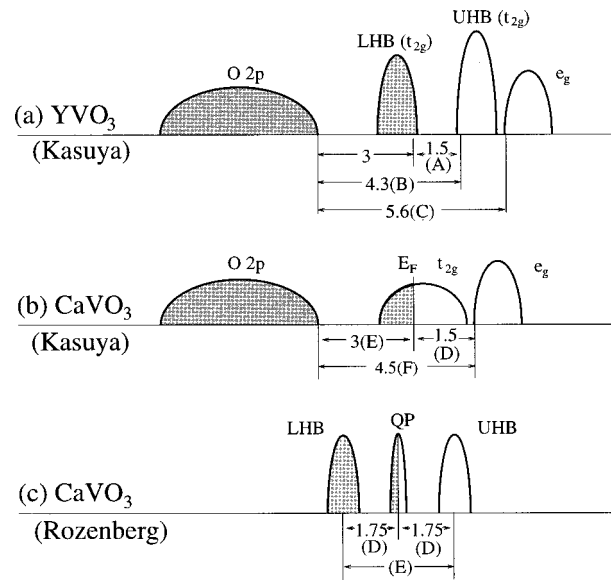


FIG. 11. Schematic densities of states of YVO_3 (a) and $CaVO_3$ (b) and (c). (a) and (b) represent the view of Kasuya *et al.*, (c) is the $d=\infty$ Hubbard picture. The energies (in eV) with their labels correspond to the peak assignments in the optical conductivity spectra of Fig. 12.

spectra (obtained from the paramagnetic solution of the $d=\infty$ Hubbard model) on decreasing U , while keeping W fixed.

Also the optical conductivity of $CaVO_3$ was described within the same model,⁴⁵ using the same parameters as for the photoemission spectra. The results are compared with $\sigma(\omega)$ data from a $CaVO_3$ single crystal, and a good agreement between theory and experiment is found. The experimental results are quite similar to those for polycrystalline material reported earlier by Kasuya *et al.*; however, the assignments made to the various spectral features are very different. In this light, it is interesting to compare the $\sigma(\omega)$ spectra of the $Y_{1-x}Ca_xVO_3$ series to our O 1s x-ray-absorption spectra. There are some remarkable similarities, which support the original assignments of Kasuya *et al.*

Let us briefly recapitulate the two different viewpoints. For YVO_3 Kasuya *et al.* take the common Mott-Hubbard picture, as shown in Fig. 11. The O $2p$ band is at a higher binding energy than the V $3d$ band, i.e., $\Delta > U$. The d states are split into upper and lower Hubbard bands by the Coulomb repulsion U , and the upper Hubbard band is further split by the crystal field in states of t_{2g} and e_g symmetry. (Note that this latter assumption is essentially not correct for a d^2 system: one has to consider not only the crystal-field interaction, but also the $d-d$ Coulomb and exchange interactions.) The thresholdlike rise in the $\sigma(\omega)$ spectrum of YVO_3 , labeled A in Fig. 12(a), is assigned to excitations across this Mott-Hubbard gap. Judging from the energy positions and the systematic variations with hole doping x , features B and C are assigned to charge transfer excitations from the O $2p$ valence state to V $3d$ states of t_{2g} and e_g symmetry, respectively. The energy difference between the Mott-Hubbard gap (~ 1.5 eV) and the charge transfer transitions (~ 4.5 eV) is in agreement with the photoemission spectrum of YVO_3 , in which the distance between the O $2p$ and V $3d$

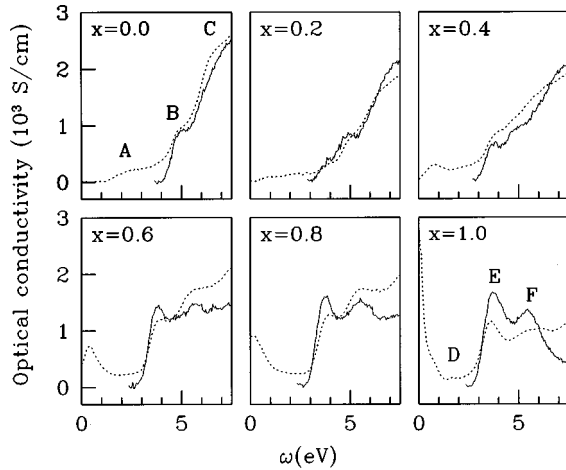


FIG. 12. Comparison of the O 1s XAS near-edge region of $Y_{1-x}Ca_xVO_3$ (solid lines) to the optical conductivity, as taken from Ref. 19.

upper band edges is about 3 eV. On increasing x , the spectral weight below 1.5 eV gradually increases, developing into a Drude edge as x approaches 1. The features above 3 eV, still assigned to charge-transfer excitations, are shifted to lower energy by about 1.5 eV compared to YVO_3 . The assignment of the high-energy spectral weight to charge-transfer excitations is consistent with the results of a comprehensive study on the optical gaps of $LaMO_3$ and YMO_3 perovskites.^{65,66} With the assignments made in this study, the trends in the gap on changing the M atom from Ti to Cu could be successfully explained within the Zaanen-Sawatzky-Allen (ZSA) framework.⁶⁷

The assignments made for the $\sigma(\omega)$ spectrum of $CaVO_3$ in the $d=\infty$ Hubbard model are quite different. Figure 11(c) schematically shows the densities of states in this model. The Coulomb interaction U , estimated at 3.5 eV from a fit to the photoemission spectrum, determines the splitting between the “incoherent” lower and upper Hubbard bands at $\omega = -1.75$ and 1.75 eV. A “coherent” quasiparticle peak is centered around $\omega=0$. The calculated $\sigma(\omega)$ spectrum yields a pronounced peak around 3.5 eV, which is attributed to transitions from the lower to the upper Hubbard band. A weak feature at around 1.75 eV, which was not discussed by Kasuya *et al.*, is assigned to excitations from the lower Hubbard band to quasiparticle states, and from quasiparticle states to the upper Hubbard band.

Figure 12 shows a comparison of $\sigma(\omega)$ to the near-edge regions of the O 1s absorption spectra. In a simple (e.g., tight-binding) band picture, the charge-transfer excitation—expected to be seen in $\sigma(\omega)$ —and the O 1s x-ray-absorption are quite similar processes. However, the O 2p band is much broader than the O 1s “band” and therefore O 1s XAS should be compared to the unoccupied DOS, while 2p-3d charge transfer should resemble the joint density of states of the O 2p and V 3d bands. Nevertheless, if the onset of the $\sigma(\omega)$ intensity corresponds to the distance between the band edges,¹⁹ it is still interesting to make the comparison. The O 1s spectra were all shifted by the same energy (-526.0 eV), in such a way that a good alignment was obtained.

The development of the near-edge features upon hole doping is very similar to that of the $\sigma(\omega)$ spectra in the

region $3 < \omega < 7.5$ eV. This supports Kasuya *et al.* assignment of the features in this region to charge-transfer excitations. For the Mott-insulating end member YVO_3 , this assignment already seems unambiguous without making the comparison with the O 1s XAS. In the first place, because of the energy positions, but also because of the intensity, $d-d$ excitations are expected to be relatively weak. On-site $d-d$ excitations are optically forbidden, and the probability for intersite excitations is small due to the small $d-d$ overlap. By overlaying the x-ray-absorption spectra, we can keep track of the development of the charge-transfer excitations in the $\sigma(\omega)$ spectra, and find that the description of Kasuya *et al.* for the $x \neq 0$ spectra is still consistent. A correspondence between optical conductivity spectra and O 1s absorption edges is also present for $La_xSr_{1-x}TiO_3$, where a double-peak structure for $SrTiO_3$ changes to a single broad peak for $LaTiO_3$.^{66,68} The onset of the $SrTiO_3$ structure is at ~ 3 eV, corresponding to the band gap,⁵³ which is definitely of charge-transfer nature.

In conclusion, we compared the optical conductivity spectra of $Y_{1-x}Ca_xVO_3$ to the O 1s absorption edges and found similar trends. These trends are consistent with Kasuya *et al.* assignments for the $\sigma(\omega)$ spectrum of $CaVO_3$, but they contradict the description by the $d=\infty$ Hubbard model.

V. CONCLUSIONS

From the photoemission spectra it is clear that the lowest electron removal states of YVO_3 ($CaVO_3$) are of predominantly $d^2 \rightarrow d^1$ ($d^1 \rightarrow d^0$) character, and $Y_{1-x}Ca_xVO_3$ can be classified in the ZSA framework to be of the Mott-Hubbard type. Nevertheless, from the fact that both the V 2p and O 1s x-ray-absorption spectra are strongly doping dependent, it can be concluded that these states are highly mixed with the O 2p ligand states. This system should thus be placed in the lower left corner of the ZSA diagram.

The V 2p spectra indicate that d electrons become delocalized on going from YVO_3 to $CaVO_3$: the $x=0$ spectrum is well described within the crystal-field multiplet model, while the $x=1$ spectrum is not. The increase in the O 1s near-edge spectral weight on going from $CaVO_3$ to YVO_3 can not be explained by rigid-band behavior. Comparison of the experimental spectra to the calculated O p projected densities of states suggest that the change in spectral weight is due to correlation effects and an increasing V-O covalence. The nonmagnetic band-structure calculations give high densities of states near E_F , in agreement with the $CaVO_3$ spectrum. The YVO_3 spectrum is better described by a magnetic calculation assuming an AFM ground state; here, the presence of local moments yields a lower DOS at E_F .

The fact that $CaVO_3$ is metallic while YVO_3 is insulating, is probably due to a decreased electron correlation (i.e., a smaller U/W ratio). There are several factors that can play a role in decreasing the band width W . The V-O covalence will increase due a shorter V-O distance and a decreasing orthorhombic distortion on going from YVO_3 to $CaVO_3$. In addition, the charge-transfer energy Δ will become smaller due to the changes in Madelung potential, which also increases the V 3d-O 2p hybridization. The decreased V-O distance can also reduce U due to the larger polarization

screening. Furthermore, the larger orbital degeneracy of the d^1 system will make ferromagnetic interactions more important compared to d^2 . This will effectively decrease U because of the smaller on-site ‘‘Hund’s rule’’ exchange energy in the excited states. It might be possible that Δ becomes smaller than U and that $CaVO_3$ therefore would be a charge transfer metal. One can ask, however, if this classification is still meaningful; because of the strong $V 3d-O 2p$ hybridization, the lowest electron removal states will be predominantly $V 3d$, with a large $O 2p$ contribution, whether Δ is larger or smaller than U .

The doping dependence of the photoemission spectra, in particular the double-peak structure of $CaVO_3$, remains an unsolved problem here. The $d=\infty$ Hubbard model has been used to explain the composition dependence of this structure in $Ca_xSr_{1-x}VO_3$. At first sight, the model gives a fairly good description of the low-energy PES—and the optical conductivity—of the $Ca_xSr_{1-x}VO_3$ series, but there are also serious problems. For PES, the model predicts a narrowing of the spectral feature near E_F instead of the observed intensity decrease. Like the $d=2$ Hubbard model, the approximation for $d=\infty$ fails to describe spectral weight transfer in systems where the number of d electrons is changed. Also the description of the optical conductivity seems problematic. Some features are assigned to $d-d$ excitations, although a charge-transfer nature is more likely when considering the

change in the optical conductivity spectra throughout the $Y_{1-x}Ca_xVO_3$ series, as well as the trends in the $LaMO_3$ and YMO_3 ($M=Ti$ to Ni) series.

The description of the metal-insulator transition in early transition-metal oxides is a very difficult problem, which is not solved here. There are several aspects which are important for early-transition oxides that could play a role in the metal-insulator transition, such as $O 2p-V 3d$ hybridization, orbital degeneracy, and strong lattice polarization. We feel that a minimum model must include at least those three interactions, and go beyond an impurity or a cluster model with only one V atom.

ACKNOWLEDGMENTS

We thank M. F. Lopez and T. Turner for assistance during the experiments. This investigation was supported by the Netherlands Foundation for Chemical Research (SON) and the Netherlands Foundation for Fundamental Research on Matter (FOM), with financial support from the Netherlands Organization for the Advancement of Pure Research (NWO), and by the ‘‘Special Coordination Fund for Promotion of Science and Technology from the Science and Technology Agency of Japan.’’ We also acknowledge a Grant-in-Aid for Scientific Research from the Ministry of Education, Science, Sports and Culture of Japan.

*Present address: Laboratorio Nacional de Luz Sincrotron, Caixa Postal 6192, Campinas, 13081-970, Brazil.

[†]Present address: Department of Physics, University of Tokyo, Bunkyo-ku, Tokyo 113-0033, Japan.

[‡]Present address: Department of Applied Physics, University of Tokyo, Bunkyo-ku, Tokyo 113-0033, Japan.

[§]Present address: Department of Superconductivity, University of Tokyo, Bunkyo-ku, Tokyo 113-0033, Japan.

¹J. G. Bednorz and K. A. Muller, *Z. Phys. B* **64**, 189 (1986).

²R. M. Kusters *et al.*, *Physica B* **155**, 362 (1989).

³S. Jin *et al.*, *Science* **264**, 413 (1994).

⁴P. D. Dernier and M. Marezio, *Phys. Rev. B* **2**, 3771 (1970).

⁵I. H. Inoue *et al.*, *Phys. Rev. Lett.* **74**, 2539 (1995).

⁶A. Fujimori *et al.*, *Phys. Rev. B* **46**, R9841 (1992).

⁷M. Abbate *et al.*, *Phys. Rev. B* **44**, 5419 (1991).

⁸C. T. Chen *et al.*, *Phys. Rev. Lett.* **66**, 104 (1991).

⁹P. Kuiper *et al.*, *Phys. Rev. Lett.* **62**, 221 (1989).

¹⁰Y. Okimoto *et al.*, *Phys. Rev. B* **51**, 9581 (1995).

¹¹K. Morikawa *et al.*, *Phys. Rev. B* **52**, 13 711 (1995).

¹²J. B. Torrance, P. Lacorre, C. Asavaroengchai, and R. M. M. Metzger, *Physica C* **182**, 351 (1991).

¹³Y. Aiura, F. Iga, Y. Nishihara, and H. Kato, *Phys. Rev. B* **47**, 6732 (1993).

¹⁴ G -type ordering is antiferromagnetic in all directions; C -type ordering is antiferromagnetic in the ab plane, and ferromagnetic in the c direction.

¹⁵H. Kawano, H. Yoshizawa, and Y. Ueda, *J. Phys. Soc. Jpn.* **63**, 2857 (1994).

¹⁶B. L. Chamberland and P. S. Danielson, *J. Solid State Chem.* **3**, 243 (1971).

¹⁷A. Fukushima *et al.*, *J. Phys. Soc. Jpn.* **63**, 409 (1994).

¹⁸H. C. Nguyen and J. B. Goodenough, *Phys. Rev. B* **52**, 8776 (1995).

¹⁹M. Kasuya *et al.*, *Phys. Rev. B* **47**, 6197 (1993).

²⁰F. Iga and Y. Nishihara, *J. Phys. Soc. Jpn.* **61**, 1867 (1992).

²¹I. Inoue *et al.*, *Physica C* **235–240**, 1007 (1994).

²²I. H. Inoue *et al.*, *Physica B* **206–207**, 850 (1995).

²³J. Zhou and J. B. Goodenough, *Phys. Rev. B* **54**, R13 393 (1996).

²⁴A. Fujimori *et al.*, *Phys. Rev. Lett.* **69**, 1769 (1992).

²⁵X. Y. Zhang, M. J. Rozenberg, and G. Kotliar, *Phys. Rev. Lett.* **70**, 1666 (1993).

²⁶D. D. Sarma, S. R. Barman, H. Kajueter, and G. Kotliar, *Physica B* **223&224**, 496 (1996).

²⁷D. D. Sarma, *Europhys. Lett.* **36**, 307 (1996).

²⁸K. Kumagai *et al.*, *Phys. Rev. B* **186–188**, 1030 (1993).

²⁹I. H. Inoue *et al.* (unpublished).

³⁰W. F. Brinkman and T. M. Rice, *Phys. Rev. B* **2**, 4302 (1970).

³¹M. Domke *et al.*, *Chem. Phys. Lett.* **173**, 122 (1990).

³²H. A. Padmore, *Rev. Sci. Instrum.* **60**, 1608 (1989).

³³O. K. Andersen and O. Jepsen, *Phys. Rev. Lett.* **53**, 2571 (1984).

³⁴O. K. Andersen, O. Jepsen, and D. Glötzel, in *Highlights of Condensed-Matter Theory*, edited by F. Bassani, F. Fumi, and M. Tosi (North-Holland, New York, 1985).

³⁵I. H. Inoue and I. Hase (private communication).

³⁶T. Mizokawa and A. Fujimori, *Phys. Rev. B* **54**, 5368 (1996).

³⁷T. Yamaguchi, S. Shibuya, S. Suga, and S. Shin, *J. Phys. C* **15**, 2641 (1982).

³⁸S. Shin *et al.*, *J. Phys. Soc. Jpn.* **51**, 906 (1982).

³⁹J. J. Yeh and I. Lindau, *At. Data Nucl. Data Tables* **32**, 1 (1985).

⁴⁰D. D. Sarma *et al.*, *Phys. Rev. Lett.* **75**, 1126 (1995).

⁴¹R. G. Egdell *et al.*, *J. Phys. C* **17**, 2889 (1984).

⁴²N. F. Mott *et al.*, *Proc. R. Soc. London, Ser. A* **345**, 169 (1975).

⁴³S. R. White *et al.*, *Phys. Rev. B* **40**, 506 (1989).

⁴⁴S. R. White, D. J. Scalapino, R. L. Sugar, and N. E. Bickers, *Phys. Rev. Lett.* **63**, 1523 (1989).

⁴⁵M. J. Rozenberg *et al.*, *Phys. Rev. Lett.* **76**, 4781 (1996).

- ⁴⁶A. Georges, G. Kotliar, W. Krauth, and M. J. Rozenberg, *Rev. Mod. Phys.* **68**, 13 (1996).
- ⁴⁷H. Kajueter, G. Kotliar, and G. Moeller, *Phys. Rev. B* **53**, R16 214 (1996).
- ⁴⁸M. Ulmke, R. T. Scalletter, A. Nazarenko, and E. Dagotto, *Phys. Rev. B* **54**, 16 253 (1996).
- ⁴⁹R. H. Wallis, N. Sol, and A. Zylbersztejn, *Solid State Commun.* **23**, 539 (1977).
- ⁵⁰B. T. Thole *et al.*, *Phys. Rev. B* **31**, 6856 (1985).
- ⁵¹D. B. Rogers *et al.*, *J. Appl. Phys.* **37**, 1431 (1966).
- ⁵²M. Abbate *et al.*, *J. Electron Spectrosc. Relat. Phenom.* **62**, 185 (1993).
- ⁵³M. Cardona, *Phys. Rev.* **140**, A651 (1965).
- ⁵⁴M. A. van Veenendaal and G. A. Sawatzky, *Phys. Rev. Lett.* **70**, 2459 (1993).
- ⁵⁵J. Fink *et al.*, *Phys. Rev. B* **32**, 4899 (1985).
- ⁵⁶J. Zaanen *et al.*, *Phys. Rev. B* **32**, 4095 (1985).
- ⁵⁷E. Pellegrin *et al.*, *Phys. Rev. B* **53**, 10 667 (1996).
- ⁵⁸H. Eskes, M. Meinders, and G. Sawatzky, *Phys. Rev. Lett.* **67**, 1035 (1991).
- ⁵⁹M. B. J. Meinders, H. Eskes, and G. A. Sawatzky, *Phys. Rev. B* **48**, 3916 (1993).
- ⁶⁰H. Eskes and G. A. Sawatzky, *Phys. Rev. B* **43**, 119 (1991).
- ⁶¹T. Saitoh *et al.*, *Phys. Rev. B* **51**, 13 942 (1995).
- ⁶²H. F. Pen, Ph.D. thesis, University of Groningen, 1997.
- ⁶³M. T. Czyżyk, R. Potze, and G. A. Sawatzky, *Phys. Rev. B* **46**, 3729 (1992).
- ⁶⁴M. Grioni, J. F. van Acker, M. T. Czyżyk, and J. C. Fuggle, *Phys. Rev. B* **45**, 4309 (1992).
- ⁶⁵T. Arima, Y. Tokura, and J. Torrance, *Phys. Rev. B* **48**, 17 006 (1993).
- ⁶⁶T. Arima and Y. Tokura, in *Spectroscopy of Mott Insulators and Correlated Metals*, edited by A. Fujimori and Y. Tokuraof, Springer Series in Solid-State Sciences (Springer, Berlin, 1995), Vol. 119.
- ⁶⁷J. Zaanen, G. A. Sawatzky, and J. W. Allen, *Phys. Rev. Lett.* **55**, 418 (1985).
- ⁶⁸Y. Fujishima, Y. Tokura, T. Arima, and S. Uchida, *Phys. Rev. B* **46**, 11 167 (1992).